ACTA CLIMATOLOGICA ET CHOROLOGICA
Universitatis Szegediensis, Tomus 47-48, 2014, 53-62

DIFFERENT ASPECTS IN THE QUANTIFICATION OF THE SKY VIEW FACTOR IN COMPLEX ENVIRONMENTS

M HÄMMERLE[1], T GÁL[2] J UNGER[2] and A MATZARAKIS[1]

[1]*Department of Meteorology and Climatology, Albert-Ludwigs-University, Werthmannstraße 10, 79085 Freiburg, Germany*
[2]*Department of Climatology and Landscape Ecology, University of Szeged, P.O.Box 653, 6701 Szeged, Hungary*
E-mail: m.haemmerle@stud.uni-heidelberg.de

Summary: This paper examines potential applications of the sky view factor (SVF) regarding two- or three-dimensional sites. First, the concepts of the radiation budget, Lambert's cosine law and hemispherical description of radiating of environments are introduced and connected to the sky view factor. Based on a comparison between different models and methods which calculate the SVF, the paper then focuses on two different kinds of SVF-calculation depending on the type of analyzed site. It is assumed that in case the point of interest represents a flat, two-dimensional area, it makes sense to include the cosine law whereas in case the point of interest represents a solid three-dimensional object the application of Lambert's law could have to be applied in another way. It is shown that the inclusion or exclusion of the cosine law results in different SVF values. It is concluded that depending on the type of surveyed area, the application of a 2D- or 3D-sky view factor should be considered in order to get a better approximation of the radiation fluxes.

Key words: sky view factor, Lambert's cosine law, radiation budget, complex environment, fish eye picture

1. INTRODUCTION

The sky view factor (SVF or ψ_s) is commonly defined as a dimensionless parameter which represents the fraction of visible sky on a hemisphere centred over the analyzed location (Oke 1981). The maximum SVF-value is 1, which occurs when the observer stands e.g. on a vast plain area or on the highest peak of a mountain range. On the opposite side, the SVF can reach a minimum value of zero which means that no sky is visible, as may be the case for a person standing in a metro station or in a very dense forest.

As the SVF changes, so do the radiation fluxes at the observed location and thus the radiation budget (Fig. 1).

Each flux-describing term of the surface radiation budget (Fig. 1) can be influenced by different settings of surface geometry when short and long wave radiation coming from the sky is replaced by radiation emitted by or radiation reflected from objects which obscure the sky (Fig. 2).

Because of the relation of sky view factor and energy balance of a surface, the SVF is widely used in studies in urban climatology (Oke 1987), biometeorology (Watson and Johnson 1988), forest climatology (Chen et al. 1991, Hale and Edwards 2002), archaeology (Kokalj et al. 2011), transport meteorology (Chapman and Thornes 2006), research on renewable energy sources (Rakovec and Zakžek 2013), urban planning (Lin et al. 2010), etc.

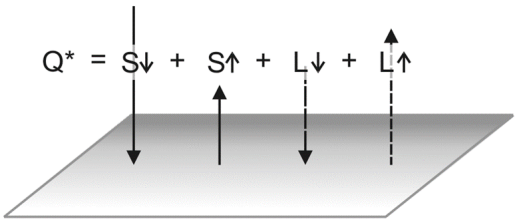

Fig. 1 Radiation budget of an "ideal" site. Q* = net radiation budget, S↓ = incoming short wave radiation (direct solar and diffuse), S↑ = outgoing short wave radiation (reflection), L↓ = incoming long wave radiation (atmospheric downward-radiation), L↑ =outgoing long wave radiation (emission of solid surfaces)

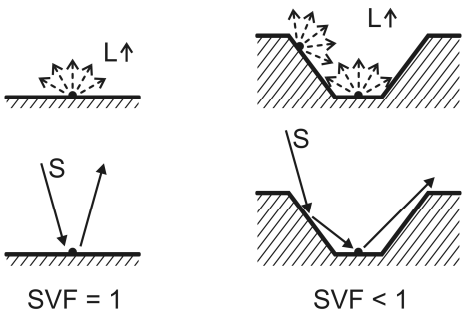

Fig. 2 Influence of horizontal (left) and convoluted (right) surfaces with accordingly different SVF values on radiation fluxes. L = long wave radiation, S = short wave radiation. (after Oke 1987)

Another definition of the sky view factor is based on radiation geometry: A view factor in general is "a geometric ratio that expresses the fraction of the radiation output from one surface that is intercepted by another. It is a dimensionless number between zero and unity" (Oke 1987). Thus the sky view factor is the geometric ratio that expresses the fraction of the radiation output from the sky that is intercepted by a surface. In this way of defining the SVF, the radiation fluxes between two-dimensional surfaces are crucial parts and thus the cosine law of Lambert has to be taken into account:

$$I = I_0 \cos(\Theta) \quad (1)$$

where I is the energy actually received at the observed location, I_0 is the energy of the original beam and Θ is the angle between the surface's normal (n, see Fig. 3) and the incoming beam. Depending on Θ, the area of interest receives thus more or less of the incoming radiation. Fig. 3 illustrates three exemplary cases and indicates the corresponding factor cos(Θ).

The application of Lambert's cosine law can also be interpreted as a weighting factor for radiation emitted by the surroundings of a certain location. If e.g. in the middle picture of Fig. 3 radiation is emitted by an object situated 30° above ground, half of the radiation flux is received at the point of interest. The extreme case would be that radiation emitted from an object which is at the same level as the point of interest, the radiation passes by and no radiation at all is received (Fig. 3 right).

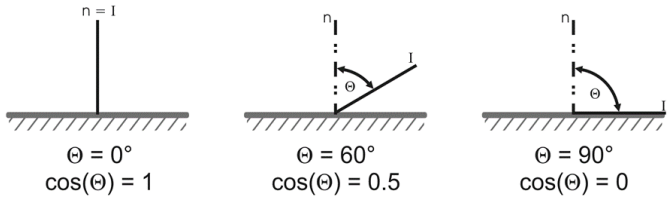

Fig. 3 Zenith angle (Θ) and the corresponding factor cos(Θ). n = surface normal, I = beam of incoming radiation

In order to get a basis for calculating the total radiation received at a certain point, the surrounding radiation sources are commonly projected onto a hemisphere which is centred at the analyzed area (Fig. 4). The angle Θ can now be described as zenith angle.

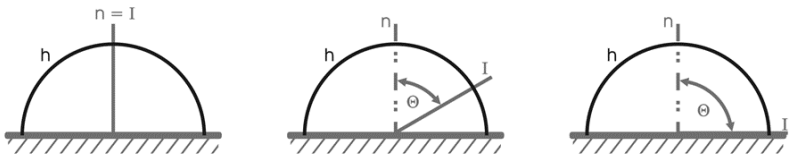

Fig. 4 Same as Fig. 3 but with a hemisphere (h) placed over the analyzed area

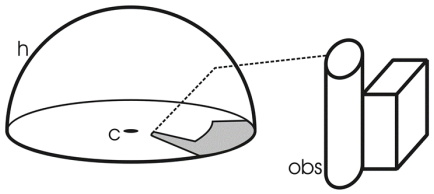

Fig. 5 Principle of projecting surroundings onto a hemisphere's (h) underlying circle. c = analyzed location in the center of the hemisphere's great circle, obs = obstacles in the perimeter obstructing the sky, grey = projection of the obstacle onto the great circle

When the radiating environment's shapes on the hemisphere are further projected onto the hemisphere's underlying circle, the result is a circular image. Fig. 5 shows a draft of a hypothetic set of buildings and their projection onto a circular picture. The analyzed location is marked with a "c", the overlying hemisphere with "h", obstacles with "obs" (Fig. 5). The path of the projection, first onto the hemisphere and then onto the hemisphere's great circle, is represented by the dashed line. As Fig. 5 is only intended to show the principle, the projection path, the shape of the projection etc. are not geometrically correct. It can be seen that the projection path breaks on the hemisphere. This break depends on and changes with the projection (e.g. equidistant, orthographic, equisolid angle) and will be ignored in the following text in order to keep the focus on the zenith angle. As the following deals with a geometrically distorted zenith angle, it will be shown as Θ'.

If one changes from an inclined view of Fig. 5 to a view vertically above the same scene, the result is (again not geometrically correct and only illustrating the principle) shown in Fig. 6.

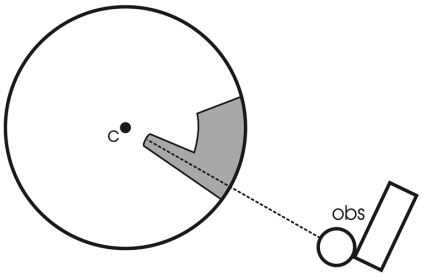

Fig. 6 Same as Fig. 5 but with a view hovering over the scene

An example image is shown in Fig 7. It was taken with fish eye lens (Nikon FC-E8) mounted on a Nikon Coolpix 4500 digital camera facing upwards.

Fig. 7 Example of a fish eye photograph. x = center of the image, arrow and Θ' = distance between image's center and obstacle

Regarding this depiction of the radiating environment, the angle Θ' basically represents the distance between the image centre (in Fig. 7 marked with a black cross) and an emitting object (in Fig. 7 exemplarily the roof's corner at which the black arrow points). Integrating the edges of radiating objects, i.e. integrating the sky line both around the circle and all over the zenith finally leads to the sky view factor as a parameter representing the radiating environment.

The objectives of this paper are to show connections between the sky view factor and Lambert's cosine law as well as to point at potential biases coming with the application of the cosine law in SVF-related calculations depending on the geometry of the analyzed point or area of interest.

2. METHODS

While evaluating the SVF for a set of pictures like the one shown in Fig. 7 as well as calculating the corresponding SVF with models using 3D databases, it was found that the SVF values differ significantly between two groups of methods and models (Hämmerle et al. 2011a). In the present study, the fish eye images were evaluated using the following methods.

Manual method according to Steyn (1980): The fish eye images were printed with an overlaying polar grid. On the print, the obstructed areas were manually delineated. Based on the delineation, the obstructed angle of each annulus was estimated and then used to calculate the sky view factor according to the formula given in Steyn (1980).

Steyn-method implemented in an ArcView Avenue-Script. The workflow is basically the same as above but the tasks are completely done on screen. The pictures do not have to be printed and delineation of the obstacles is done by digitizing the obstacle's shapes in a GIS (Hämmerle et al. 2011b).

RayMan-model (Matzarkis et al. 2007): This model includes the "Edit free sky view factor"-tool which calculates the SVF from fish eye pictures or any other circular images with distinct obstacles. In order to determine the SVF on the basis of a fish eye picture, the image is loaded into the "Edit free sky view factor"-tool. After that, the obstacles are digitized on screen. The tool then counts the sky pixels and relates them to the overall number of pixels in the image. As an alternative to fish eye images taken with a digital camera, obstacle files can be loaded into the tool. A fish eye image is then produced which can also be used for deriving the sky view factor of the scenery modelled in the obstacle file.

BMSkyView (Rzepa and Gromek 2006): This software selects sky pixels according to their similarity in color. Sky pixels are selected manually and then, depending on the chosen threshold, all similar pixels in the image are classified also as sky. Misclassifications (caused e.g. by reflecting windows) are corrected manually. The selected sky pixels finally form the basis for calculating the SVF via the formula in Steyn (1980).

The SVF values presented in the results of this study were calculated by the following software methods. For the input of these software we used a 3D building data base of Szeged, southern Hungary, as described in Unger (2006).

SkyHelios (Matzarakis and Matuschek 2010): This model calculates the SVF for a whole area. In SkyHelios, obstacle-files as well as shape-files can be loaded. Using the computer's video card, fish eye images are produced for each point in the area of interest. Based on the fish eye images, the SVF is calculated for each point. The result is a set of equally distant points with an SVF-value generated for each point.

ArcView SVF-Extension (Gál et al. 2009): This script was developed in the proprietary Avenue script language which is implemented in ESRI ArcView. The script works with a shape file containing the footprints and heights of buildings. From each point of interest, the horizon is scanned for obstacles, i.e. buildings. If an obstacle is hit, its elevation angle is calculated based on the height data read from the data base. The SVF is calculated for the same points based on the highest elevation angle in each direction. The highest obstacle in the scanned direction is taken for SVF-calculation. The scanning range and angular step width can be selected depending on the available computing power and time.

The SOLWEIG-model (Lindberg et al. 2008) based on a shadow casting algorithm as described in Ratti and Richens (1999). A virtual hemisphere, equipped with light sources, is placed over each point of interest. A DSM containing the obstacles is loaded into the model, partially obstructing the hemisphere. The value of the SVF is calculated based on the number of obstructed light sources.

As the original shape files of the 3D building data base cannot be processed directly with RayMan, the shape file had to be converted to the obstacle file format of RayMan before calculating. The footprints of the buildings in the obstacle file have to be convex quadrilateral.

For the conversion a script is developed using ArcView GIS system's built-in object-oriented script language (Avenue). The script uses the fact that all of the polygons can be split into triangles using the rule that triangles have to be convex. The script divides the buildings' polygons within a user defined distance from a selected centre point iterative into triangles. The result is stored in a text file which satisfies the criteria of the obstacle file format. The maximum number of iterations can be changed before the calculation, because the conversion of the more complex polygon shapes in some cases needs a higher number of runs. After splitting the polygons, a new vertex is inserted into the longest side of each triangle in order to meet the expectations of the obstacle file format. The building's relative height is calculated using the elevation of the top of the building and the elevation of the center point of the area. The output of the script can be used directly as input for the RayMan model. Vegetation can also be converted by this script. This Avenue-script and additionally, a Python plug-in for QGIS are freely available and is available from the authors on request.

Fig. 8 shows a resulting obstacle file loaded in RayMan. The obstacle file shown in Fig. 8 contains all buildings within an area of 400 x 400 m and the point of interest as centre point. The centre of the scene in Fig. 8, where the line S-N and E-W cross, corresponds to point 3033 of the transect through an urban neighbourhood that is analysed in this study.

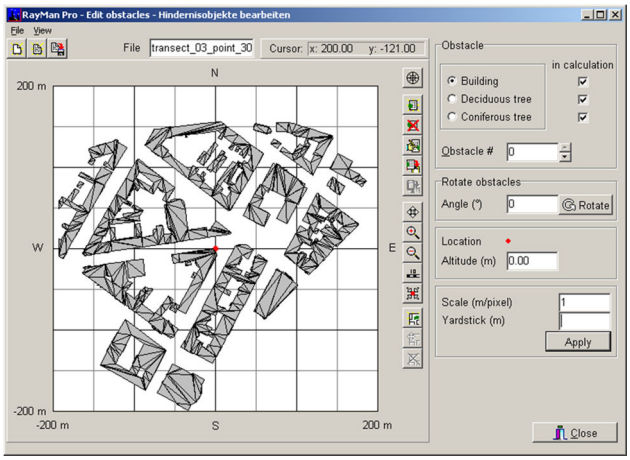

Fig. 8 RayMan Pro-interface showing an obstacle-file derived from a shape-file. Red point: analyzed point, grey: surrounding buildings in obs-format

3. EXEMPLARY RESULTS

Fig. 9 gives as an example the development of the SVF-values along a straight transect of 19 equidistant points (0.5 m) within an urban setting (for more details see Hämmerle et al. 2011a). The images were taken from ground level on a y-shaped intersection of three streets with a Nikon Coolpix 4500 digital camera and a Nikon Fisheye Converter FC-E8 0.21x mounted on a Gorillapod original tripod supplementary equipped with a bubble level. The surrounding buildings are up to 15 meters high except one building of some 30 meters north-east of the transect. Vegetation in leaf-on phase was covering the sky only to a very small

part and was manually eliminated in the models using fish-eye pictures. Fig. 7 corresponds to point 3033 in the given diagram.

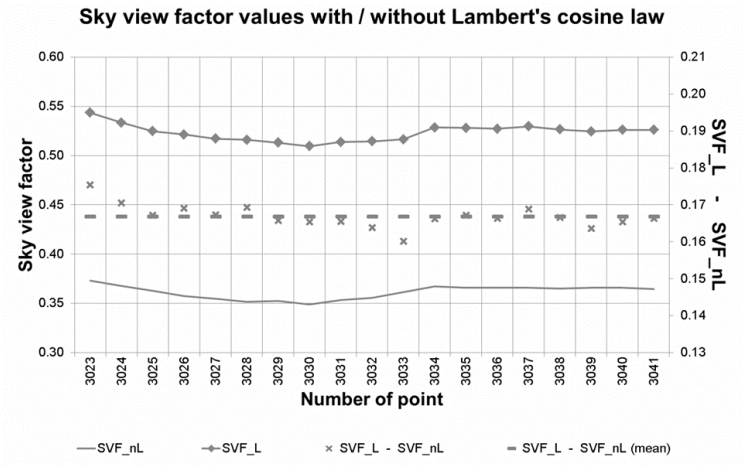

Fig. 9 SVF-values along an urban canyon, calculated with different methods. X-axis: single points of transect, left y-axis: SVF for each point, right y-axis: difference between SVF-values derived from models with applied cosine-law (SVF_L-line) and SVF-values derived from models without Lambert's law (SVF_nL-line). Crosses: Difference SVF_L - SVF_nL for each point, dashed line: mean of all differences

The different SVF-values turned out to be influenced by taking into account Lambert's cosine-law or not (Hämmerle et al. 2011a). In Fig. 9, the lower line (SVF_nL, for "SVF no Lambert") shows the mean SVF-value coming from three methods: RayMan, SkyHelios with vector input, SkyHelios with raster input. The upper line (SVF_L) includes all seven used methods and shows again the mean SVF of the seven values. This time, Lambert's cosine law was applied by RayMan and SkyHelios. The difference between the lower and upper line (i. e. SVF_L – SVF_nL) for each point is marked with an "x" in the diagram. The dashed line shows the average of all differences.

The reason for the higher SVF-values when applying Lambert's cosine law is to be found in the strong emphasis of the area around the zenith or respectively the lower weight of objects obstructing the sky at the horizon. Illustrating this dependence, fig. 10 shows the sky view factor for different heights over point 3033 (corresponding fish eye picture in Fig. 7). On the basis of the 3D building data base as described in Gál et al. (2009) the SVF was calculated in steps of 0.25 Meters from ground level to 25 Meters above ground. One calculation was done in ArcView using the ArcView SVF-Extension (Gál et al. 2009), two other runs were made with RayMan (Matzarakis et al. 2007).

The results of the three SVF-calculations for different heights on and above point 3033 are shown in Fig. 10.

The left curve in Fig. 10 (RayMan-weight) shows the SVF-values for the RayMan-calculation without the weight according to Lambert's cosine-law. The other two curves (RayMan+weight, ArcView+weight) result from SVF-calculations which apply the cosine-weighting. In all the three cases, especially in the first 15 meters of the vertical transect, the sky view factor is lower. At the height of about 15 meters the sky starts to open and

accordingly the SVF increases. After emerging from the street canyon only a few higher buildings obstruct the sky but they appear very low on the horizon. Fig. 11 shows a sequence of 5 fish eye images generated with RayMan for five different heights. The sun path in the fish eye images is inserted automatically by RayMan but are not of interest for this study.

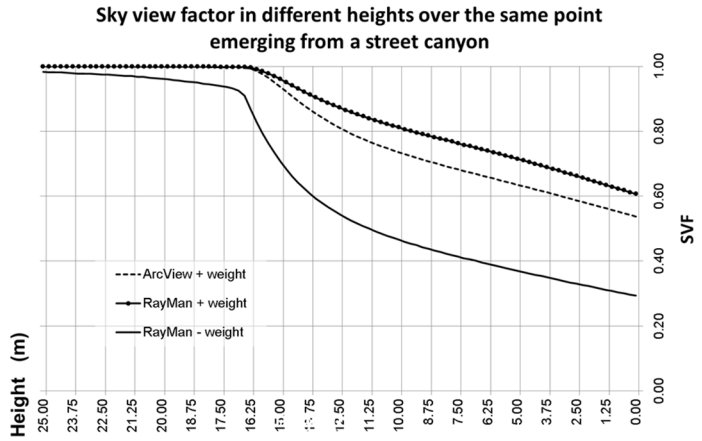

Fig. 10 SVF-values for successive heights above a fixed point, calculated with different methods. Y-axis: height of SVF-calculation, x-axis: SVF-range, solid line: SVF-value at different heights calculated with RayMan not applying the cosine-law, dashed line and solid line with points: SVF-value at different heights calculated with RayMan and ArcView with applied cosine-law

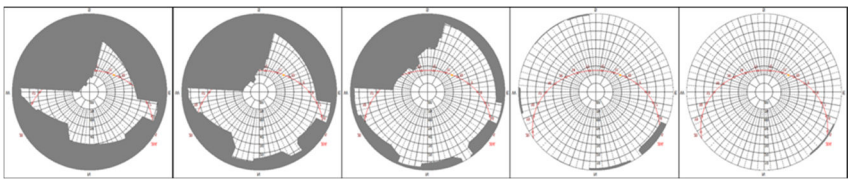

Fig. 11 RayMan-generated fish eye pictures for the same position but with different heights (left to right: 0.00 m, 6.25 m, 12.50 m, 18.75 m, 25.00 m). Grey: surrounding buildings, polar diagram: indicating open sky, red line: sun path

The SVF-values for the heights above 15 meters emphasize the different weighting of objects obstructing the lower parts of the horizon (Figs. 10 and 11). If Lambert's cosine law is not applied (left curve in Fig. 10), the still obstructing buildings are taken into account and a SVF of 1 is not reached. On the other hand, weighting the objects according to Lambert's Law leads to a sky view factor of 1 starting from about 16 meters height (central and right curves in Fig. 10).

3. DISCUSSION

The question comes up why in some models the cosine-law was included and why not in others. The reason most likely lies in the way of defining the area of interest: As long as a point or a two-dimensional area like a square is regarded, Lambert's law can be applied

without restrains. But what happens if a 3D object like a person is placed in a radiating environment and the radiation received by this object is of central interest? Fig. 12 illustrates this case by simply putting a cylinder (representing approximately the shape of e.g. a person as proposed in Johnson and Watson 1984, Höppe 1984) into Fig 4.

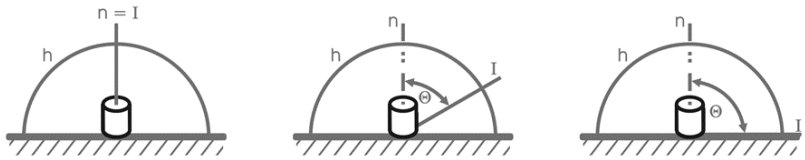

Fig. 12 Cosine-weighting and its influence on radiation received by a solid object (same as fig. 4 but with an object placed in the hemisphere's center)

If Lambert's cosine law is applied here in the standard way, all fluxes received by non-horizontal areas are calculated as too low. In case of radiation parallel to the horizon (right part of Fig. 3) the object would not receive any radiation at all if the cosine-weighting is applied because of $\Theta = 90°$.

Thus it seems necessary to discuss the definition of the sky view factor depending on the aim of an analysis: Is the point of interest a flat area or is it an object whose radiation fluxes are of central concern? Should there accordingly be defined a SVF_{2D} which includes Lambert's cosine-law and on the other hand a SVF_{3D} with an adaption of the weighting appropriate for solid objects? How could a comprehensive implementation be found of the extremely complex matter of how to weight all radiation fluxes received by a 3D object and the surfaces it consists of? How to deal with different wave-lengths, the distinction between direct and diffuse short wave radiation and the different components of the radiation budget? How to include the sun path in connection with the date and latitude of the point or object of interest?

3. CONCLUSION

In this paper the cosine law according to Lambert was introduced and connected to hemispherical photography and the sky view factor. It was found that with different settings the application of Lambert's cosine law can lead to different results. The question came up whether Lambert's cosine law should be applied or not depending on the type of the analyzed area or object. In case a study deals with a flat area, the cosine law seems according to our results straightforward and offers an established way of taking angle-dependent radiation fluxes into account. On the other hand in case the study deals with solid three-dimensional objects, the application of Lambert's cosine law may lead to biased results. The question of introducing two types of SVF, one for a 2D-setting, the other for a 3D-setting, should be discussed intensively in order to improve the quality and reliability of studies in all concerned research in e.g. urban climatology and in the various branches of biometeorology.

Acknowledgements: The study was supported by the Hungarian Scientific Research Fund (OTKA PD-100352).

REFERENCES

Chapman L, Thornes JE (2006) A geomatics based road surface temperature prediction model. Sci Total Environ 360:68-80

Chen JM, Black AT, Adams RS (1991) Evaluation of hemispherical photography for determining plant area index and geometry of a forest stand. Agr Forest and Meteorol 56:129-143

Gál T, Lindberg F, Unger J (2009) Computing continuous sky view factors using 3D urban raster and vector databases: comparison and application to urban climate. Theor Appl Climatol 95:111-123

Hala SE, Edwards C (2011) Comparison of film and digital hemispherical photography aross a wide range of canopy densities. Agr Forest and Meteorol 112:51-56

Hämmerle M, Gál T, Unger J, Matzarakis A (2011a) Comparison of models calculating the sky view factor for urban climate investigations. Theor Appl Climatol, 105:521-527

Hämmerle M, Gál T, Unger J, Matzarakis A (2011b) Introducing a script for calculating the sky view factor used for urban climate investigations. Acta Climatologica et Chorologica Univ Szegediensis, 44-45:83-92

Höppe P (1984) Die Energiebilanz des Menschen. Wiss Mitt Met Inst Univ München, München

Johnson GT, Watson ID (1984) Person view-factors in the urban environment. Arch Meteor Geophy B 34:273-285

Kokalj Ž, Zakšek K, Oštir K (2011) Application of sky-view factor for the visualisation of historic landscape features in lidar-derived relief models. Antiquity 85:263-273

Lin TP, Matzarakis A, Hwang RL (2010) Shading effect on long-term outdoor thermal comfort. Build Environ, 45:213-221

Lindberg F, Thorsson S, Holmer B (2008) SOLWEIG 1.0 - Modelling spatial variations of 3D radiant fluxes and mean radiant temperature in complex urban settings. Int J Biometeorol 52:697-713

Matzarakis A, Matuschek O (2010) Sky view factor as a parameter in applied climatology − rapid estimation by the SkyHelios model. Meteorol Z 20:39-45

Matzarakis A, Rutz F, Mayer H (2007) Modeling radiation fluxes in simple and complex environments - application of the RayMan model. Int J Biometeorol 51:323-334

Oke TR (1981) Canyon geometry and the nocturnal urban heat island. Comparison of scale model and field observations. J Climatol 1:237-254

Oke TR (1987) Boundary layer climates. Methuen, London

Rakovec J, Zakžek K (2013) On the proper analytical expression for the sky-view factor and the diffuse irradiation of a slope for an isotropic sky. Renew Energ 37:440-444

Ratti C, Richens P (1999) Urban texture analysis with image processing techniques. In: Augenbroe G, Eastman Ch (eds) Proceed 8th Int Confon Computer Aided Architectural Design Futures held in Atlanta, Georgia

Rzepa M, Gromek B (2006) Variability of sky view factor in the main street canyon in the center of Łódź. Preprints Sixth Int Conf on Urban Climate, Göteborg, Sweden. 854-857

Steyn DG (1980) The calculation of view factors from fisheye-lens photographs. Atmos Ocean 18:245-258

Unger J (2004) Intra-urban relationship between surface geometry and urban heat island: review and new approach. Climate Res 27:253-264

Watson ID, Johnson GT (1988) Estimating person view-factors from fish-eye lens photographs. Int J Biometeorol 32:123-128